Optimized Controller Gains Using Grey Wolf Algorithm for Grid Tied Solar Power Generation with Improved Dynamics and Power Quality

Veramalla Rajagopal[1*], *Danthurthi Sharath*[1], *Gundeboina Vishwas*[1], *Jampana Bangarraju*[2], *Sabha Raj Arya*[3] *and Challa Venkatesh*[1]

(1. Department of Electrical and Electronics Engineering,
Kakatiya Institute of Technology and Science Warangal, Telangana 506015, India;
2. Department of Electrical and Electronics Engineering,
B V Raju Institute of Technology, Telangana 502313, India;
3. Department of Electrical Engineering,
Sardar Vallabhbhai National Institute of Technology Surat, Gujarat 395007, India)

Abstract: This study proposes a control algorithm based on synchronous reference frame theory with unit templates instead of a phase locked loop for grid-connected photovoltaic (PV) solar system, comprising solar PV panels, DC-DC converter, controller for maximum power point tracking, resistance capacitance ripple filter, insulated-gate bipolar transistor based controller, interfacing inductor, linear and nonlinear loads. The dynamic performance of the grid connected solar system depends on the effect operation of the control algorithm, comprising two proportional-integral controllers. These controllers estimate the reference solar-grid currents, which in turn generate pulses for the three-leg voltage source converter. The grey wolf optimization algorithm is used to optimize the controller gains of the proportional-integral controllers, resulting in excellent performance compared to that of existing optimization algorithms. The compensation for neutral current is provided by a star-delta transformer (non-isolated), and the proposed solar PV grid system provides zero voltage regulation and eliminates harmonics, in addition to load balancing. Maximum power extraction from the solar panel is achieved using the incremental conductance algorithm for the DC-DC converter supplying solar power to the DC bus capacitor, which in turn supplies this power to the grid with improved dynamics and quality. The solar system along with the control algorithm and controller is modeled using Simulink in Matlab 2019.

Keywords: Control algorithm, solar power generation, DC-DC converter, star-delta transformer, maximum power point tracking, power quality, grey wolf optimization algorithm

1 Introduction

Motivation and Incitement: The primary challenge facing existing power system networks is global warming and the emission of greenhouse gases resulting from fossil fuel and coal combustion. Hence, an intelligent, efficient, effective, robust, safe, and environmentally friendly smart power generation system is required.

Literature review: This section discusses the applications of solar power generation technology and the design and implementation of solar technologies that are typically not considered, such as solar water pumping, distillation, detoxification, refrigeration, and rural electrification [1]. Murphy et al. [2] evaluated the feasibility of using alternative water resources to meet water demands for utility-scale solar energy development, focusing on solar energy and competitive renewable energy zones. This enables generation of power from renewable sources such as wind and solar. Solar power is a clean, limitless, and environmentally friendly energy source. However, despite its continuous supply, its interconnection to grid-solar systems faces several challenges such as

Manuscript received June 7, 2021; revised September 20, 2021; accepted December 29, 2021. Date of publication June 30, 2022; date of current version May 11, 2022.
* Corresponding Author, E-mail: vrg.eee@kitsw.ac.in
Digital Object Identifier: 10.23919/CJEE.2022.000016

reliability, power quality, performance, and energy conversion cost [3-5]. Any interconnected grid should meet such power quality standards to be compliant with IEC and IEEE 519 standards [6-7]. Bhattacharya et al. [8] proposed the synchronous reference frame (SRF) theory for a hybrid series active filter system. Singh et al. [9] proposed the power balance theory algorithm for active filters and experimentally investigated the design and development of an active filter. Bhuvaneswari et al. [10] proposed a novel Icosφ algorithm applied to a three-phase shunt active filter to provide harmonics and reactive power compensation for a nonlinear reactive load. Bojoi et al. [11] proposed a single-phase inverter for distributed generation (DG) systems requiring power quality features, such as harmonic and reactive power compensation for grid-connected operation. The aim was to integrate the DG unit functions with shunt active power filter capabilities. Bangarraju et al. [12] proposed new and simplified unit templates instead of a standard phase locked loop (PLL) for an SRF control algorithm. The extraction of synchronizing components ($\sin\theta$ and $\cos\theta$) for parks and inverse parks transformation using standard PLL requires longer execution time. Bratcu et al. [13] investigated global power optimization for cascaded dc-dc converter architectures of photovoltaic (PV) generators irrespective of the irradiance conditions. The global optimum of such connections of PV modules is typically equivalent to performing the maximum power point tracking (MPPT) on all the modules. Ghasemi et al. [14] proposed a method to obtain the global maximum power point in a deterministic and fast manner. It intelligently takes some samples from the *P*-*V* curve of the array as input and divides the search voltage range into small subregions. Subsequently, it approximates the *I*-*V* curve of each subregion with a simple curve and estimates an upper limit for the array power in that subregion accordingly. Hua et al. [15] presented an improved solar system with MPPT, in which a digital signal processor is used to control the converter with the proposed control; thus, the system can implement MPPT independently for each solar panel, regardless of whether it is under shading or irradiation conditions, or contains faulty solar cells. Mirjalili et al. [16] proposed a novel meta-heuristic called the grey wolf optimizer (GWO) inspired by grey wolves. The GWO algorithm mimics the leadership hierarchy and hunting mechanism of grey wolves in nature and four types of grey wolves such as alpha, beta, delta, and omega are employed to simulate the leadership hierarchy. Li et al. [17] presented a comprehensive introduction to the GWO algorithm. They performed numerical experiments on four benchmark functions and applied them to the synthesis of linear arrays to reduce the peak sidelobe level under various constraints. Finally, the performance of the GWO was further verified on the optimization design of two representative antennas, namely, dual-band E-shaped patch and wideband magneto-electric dipole antennas. Rashidi et al. [18] optimized the structure using the multi-objective GWO to maximize the effective mode area and bending loss of higher-order modes, while minimizing the fundamental mode loss. The various control algorithms that use Ziegler and Nichols tuning method to estimate K_p and K_i gains for proportional-integral (PI) controllers and require settling time for dynamics have limitations. Grey wolf optimization provides better K_p and K_i values over conventional evolution algorithms. The unit template-based SRF algorithm is modified in combination with the grey wolf optimization technique (GWOT), allowing the flow of active power to the grid with increased power efficiency. Elgendy et al. [19] proposed an efficient and cost-effective incremental conductance MPPT algorithm to improve the energy utilization efficiency of low-power PV systems.

Contribution and organization of this paper: The rapid depletion of fossil fuels and increasing demand for electrical energy have led to the use of solar energy for power generation. The integration of solar power, which is environmentally friendly, into the grid with improved power quality and dynamics is the contribution of this study. The control algorithm is a key component of the grid-connected solar system and is used to estimate the reference source currents. The estimation of reference source currents depends on the gains of AC and DC PI controllers when optimized for better dynamics and improved power quality.

The grey wolf optimization algorithm is used to determine the gains of PI controllers; the cost function is added before the PI controller. The errors of the DC

and AC PI controllers are (i) summed (integral), (ii) squared, and (iii) time-weighted, referred to as integral of time-weighted squared error (ITSE), to optimize the gains of DC and AC PI controllers.

2 System configuration and operation

Fig. 1 shows the grid-solar system to improve system dynamics and power quality. The system consists of series-parallel-connected solar PV panels, DC-DC converters (between the controller and the solar panels), three AC interfacing inductors, and controllers (operating with unit template-based SRF control algorithm). Solar PV system output operated at maximum power point uses an algorithm based on incremental conductance, which generates a duty cycle for the DC-DC converter to supply solar power to the DC bus that is maintained at 800 V. A star-delta-connected non-isolated transformer compensates for the neutral current by connecting the transformer neutral and load. Controllers are used in solar grid-connected systems to offer the same functional capabilities as shunt active compensators along with solar power pumping into the grid. The main objectives are to achieve load balancing, harmonics reduction, load neutral current suppression, and reactive power supply. The quick response depends on the gains of AC and DC PI controllers and they are optimized using the grey wolf optimization algorithm. The system data are listed in Tabs. 1-3.

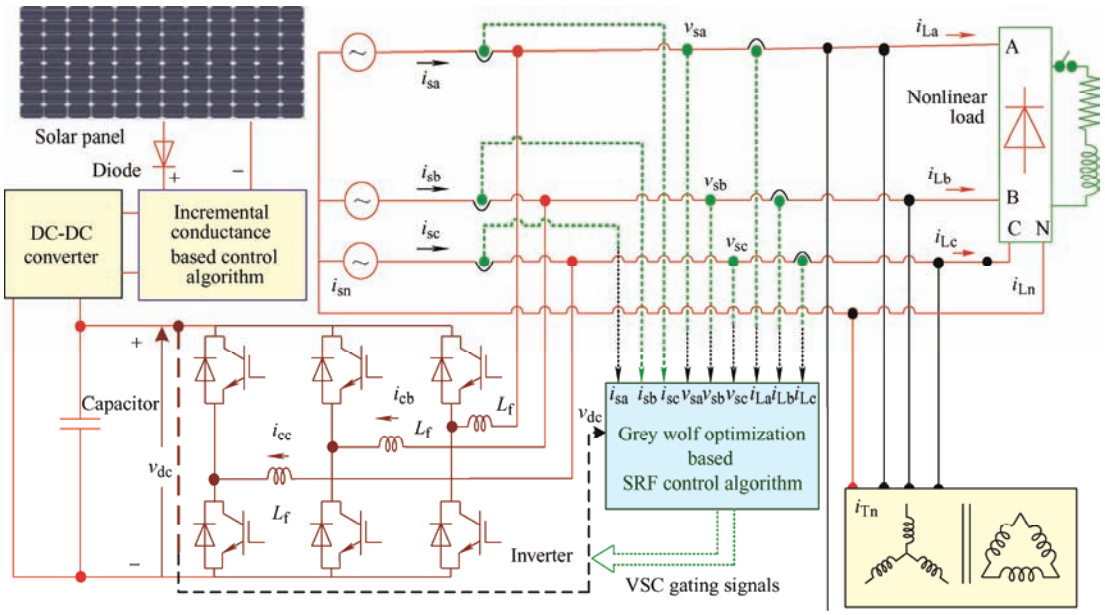

Fig. 1 Schematic of the proposed system

Tab. 1 Solar module parameters

Parameter	Value
No of series PV cells	84
V_{oc}/V	64.8
I_{sc}/A	7.8
R_s/Ω	0.18
R_p/Ω	360
No. of series modules	13
No. of parallel modules	66

Tab. 2 Irradiance and temperature

S. No	Time/s	Irradiance/(W/m^2)	Temperature/℃
1	0-1	500	20
2	1-2	750	30
3	2-3	1 000	40
4	3-4	1 000	40

Tab. 3 System parameters

S. No	Parameter	Value
1	Grid voltage	415 V, 50 Hz
2	DC-bus capacitor/μF	3 500
3	Interfacing inductor/mH	2.9
4	RC filter	10 Ω and 20 μF
5	Star-delta transformer	10 kV • A, 240/240 V
6	Switching frequency/kHz	10
7	Non-linear loads	Diode bridge rectifier with 20 Ω and 500 mH
8	Linear loads	10 kV • A, 0.8 pf lag
9	GWO	10 iterations and 5 search agents
10	Sample time/μs	10

Figs. 2a-2b show *I-V* and *P-V* curves of solar modules, with 13 series panels for acquiring solar PV

voltage (V_{sol}) and 66 parallel strings for acquiring solar PV current (I_{sol}), to obtain solar PV power (P_{sol}) at different temperatures and irradiation levels. Fig. 2c show the variation of temperature and irradiance with time.

Solar PV power regulation has three distinct algorithms. First, the unit templates-based SRF control algorithm extracts reference currents intended for the controller. Second, the peak power of the PV solar system can be obtained by applying the incremental conductance algorithm to generate a duty cycle for the DC-DC converter. Finally, optimized controller proportional-integral gains can be obtained using the grey wolf optimization algorithm.

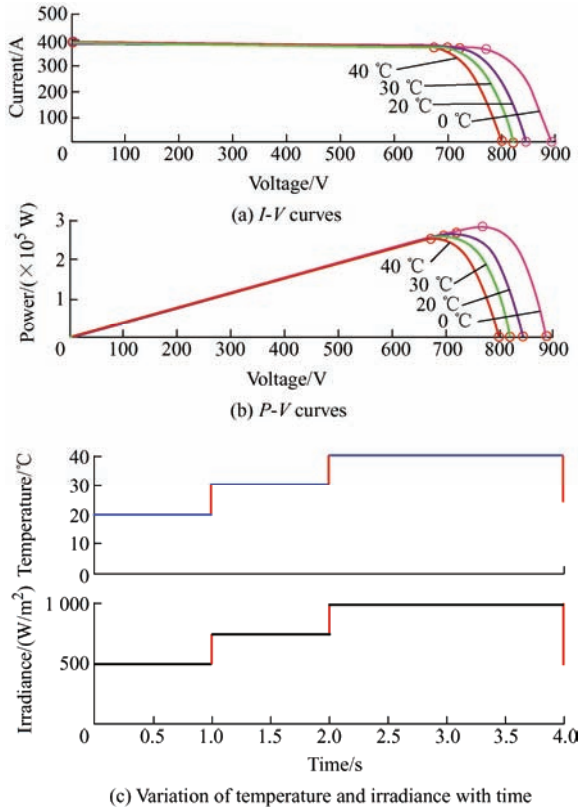

Fig. 2 *I-V* curves, *P-V* curves, variation of temperature and irradiance with time

3 Unit template-based SRF control algorithm

Fig. 3 shows the unit template (UT)-based SRF control algorithm to generate sinθ and cosθ for grid-tied solar systems. The controller is intended for harmonics exclusion, voltage regulation, and neutral current compensation. Reference source currents are extracted as follows: Using the park transformation Eq. (1), the load currents are transformed from the *a-b-c* to *d-q-o* axis.

$$\begin{bmatrix} i_{dL} \\ i_{qL} \\ i_{oL} \end{bmatrix} = \frac{2}{3}\begin{bmatrix} \sin\theta & \sin(\theta-120^{o}) & \sin(\theta+120^{o}) \\ \cos\theta & \cos(\theta-120^{o}) & \cos(\theta+120^{o}) \\ 0.5 & 0.5 & 0.5 \end{bmatrix}\begin{bmatrix} i_{La} \\ i_{Lb} \\ i_{Lc} \end{bmatrix} \quad (1)$$

where sinθ and cosθ are extracted from voltage sources (v_{sa}, v_{sb}, v_{sc}) in the system, which reduces the computational burden on the controller compared to three-phase PLLs. w_{pa}, w_{pb}, and w_{pc} are in-phase unit templates analogous to sinθ. The w_{qa} quadrature-phase unit templates are analogous to cosθ.

$$w_{pa}=\frac{v_{sa}}{v_{tg}} \qquad w_{pb}=\frac{v_{sb}}{v_{tg}} \qquad w_{pc}=\frac{v_{sc}}{v_{tg}} \quad (2)$$

$$w_{qa}=-\frac{w_{pb}}{\sqrt{3}}+\frac{w_{pc}}{\sqrt{3}} \quad (3)$$

where v_{tg} is the magnitude of the terminal voltage for the solar PV system and is expressed as

$$v_{tg}=0.816\sqrt{(v_{sa}^{\ 2}+v_{sb}^{\ 2}+v_{sc}^{\ 2})} \quad (4)$$

The DC bus voltage for the self-supported compensator is controlled using a DC bus PI controller.

$$i_{pls(k)}=i_{pls(k-1)}+K_{p1}(v_{ep(k)}-v_{ep(k-1)})+K_{i1}v_{ep(k)} \quad (5)$$

where $V_{ep}=V_{dc}^{*}-V_{dc}$. The current loss variable (i_{pls}) is the deviation of reference v_{dc}^{*} from the actual v_{dc}, and the k^{th} sample moment is assumed as v_{ep}.

The PI control gains of the DC bus are K_{p1} and K_{i1}. This current loss component (i_{pls}) is added to the direct-axis part of the DC load current (i_{dL}) to acquire the *d*-axis source part DC current (i_{dL}^{*}). The *d*-axis of the source current (i_{dL}^{*}) is expressed as

$$i_{dL}^{*}=i_{dL}+i_{pls} \quad (6)$$

The difference between the reference magnitude of the terminal voltage (V_{tr}) and the actual magnitude of the terminal voltage (V_{tg}) of the AC PI controller and its error voltage (v_{etg}) at the k^{th} sample is expressed as

$$v_{etg(k)}=v_{tg(k)}^{*}-v_{tg(r)} \quad (7)$$

$$i_{qls(k)}=i_{qls(k-1)}+k_{p2}(v_{etg(k)}-v_{etg(k-1)})+k_{i2}v_{etg(k)} \quad (8)$$

The PI control gains of the AC PI controllers are K_{p2} and K_{i2}. This current loss part (i_{qls}) is added to q-part of the load current (i_{qL}) to obtain the source component current (i^*_{qL}) of the q-axis.

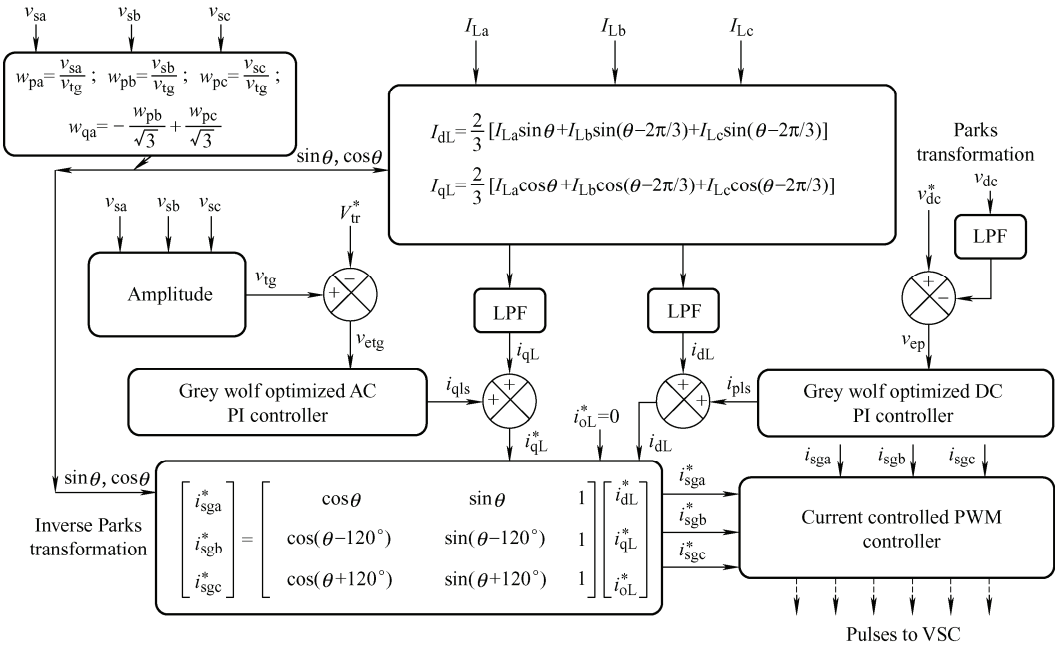

Fig. 3 UT-based SRF control algorithm for solar PV systems

The q-axis part of the source current (i^*_{qL}) is expressed as

$$i^*_{qL} = i_{qL} + i_{qls} \tag{9}$$

Using inverse park transformation, the d-q-o to a-b-c for reference grid currents (i^*_{dL}, i^*_{qL}, i^*_{oL}) are transformed to reference grid currents (i^*_{sga}, i^*_{sgb}, i^*_{sgc}).

$$\begin{bmatrix} i^*_{sga} \\ i^*_{sgb} \\ i^*_{sgc} \end{bmatrix} = \begin{bmatrix} \cos\theta & \sin\theta & 1 \\ \cos(\theta-120^\circ) & \sin(\theta-120^\circ) & 1 \\ \cos(\theta+120^\circ) & \sin(\theta+120^\circ) & 1 \end{bmatrix} \begin{bmatrix} i^*_{dL} \\ i^*_{qL} \\ i^*_{oL} \end{bmatrix} \tag{10}$$

The reference grid currents of the solar PV grid (i^*_{sga}, i^*_{sgb}, i^*_{sgc}) are subtracted from sensed source currents (i_{sga}, i_{sgb}, i_{sgc}) and the errors of grid currents (i_{sgea}, i_{sgeb}, i_{sgec}) are fed into the PWM generator to produce three-leg VSC switching pulses.

4 Incremental conductance algorithm

The incremental conductance algorithm evaluates the variance path of the instantaneous power of solar modules for incremental conductance by calculating and comparing it with its previous value. If the value ($\mathrm{d}I_{pv}/\mathrm{d}V_{pv}$) equals ($-I_{pv}/V_{pv}$), it implies that the maximum power point (MPP) is reached [17-18]. The P-V curve for the solar module is shown in Fig. 4.

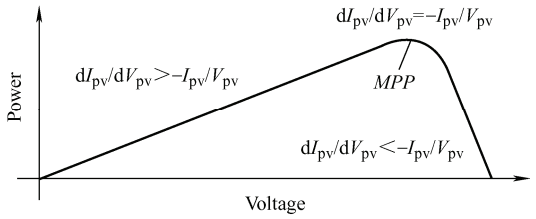

Fig. 4 P-V curve

$$\frac{\mathrm{d}P_{pv}}{\mathrm{d}V_{pv}} > 0 \text{, at the left side of the MPP} \tag{11}$$

$$\frac{\mathrm{d}P_{pv}}{\mathrm{d}V_{pv}} = 0 \text{, at MPP} \tag{12}$$

$$\frac{\mathrm{d}P_{pv}}{\mathrm{d}V_{pv}} < 0 \text{, at the right side of MPP} \tag{13}$$

$$\frac{\mathrm{d}P_{pv}}{\mathrm{d}V_{pv}} = \frac{\mathrm{d}(I_{pv}V_{pv})}{\mathrm{d}V_{pv}} = V_{pv}\frac{\mathrm{d}I_{pv}}{\mathrm{d}V_{pv}} + I_{pv}\frac{\mathrm{d}V_{pv}}{\mathrm{d}V_{pv}} = V\frac{\mathrm{d}I_{pv}}{\mathrm{d}V_{pv}} + I_{pv} \tag{14}$$

Using the above equation $\mathrm{d}P/\mathrm{d}V=0$ can be written as $\mathrm{d}I/\mathrm{d}V=(-I/V)$. Where $\mathrm{d}V$ and $\mathrm{d}I$ represent the error voltage and current after and before the incremental change, respectively. The flowchart of the MPPT incremental conductance algorithm is shown in Fig. 5.

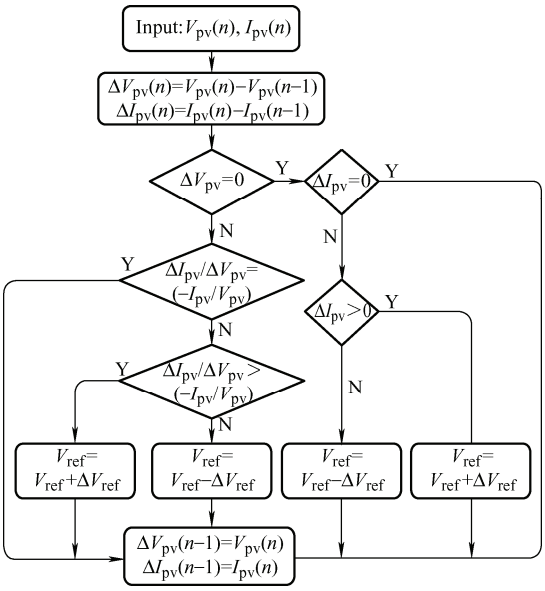

Fig. 5 Conductance-based MPPT solar PV system

5 Grey wolf optimization technique

The GWOT mimics the hunting and hierarchical mechanism of grey wolves (Canis lupus) available in nature. The best solution obtained is considered alpha (α), the second-best solution as beta (β) and delta (δ), and the third-best solution as omega (ω).

The mathematical model behavior of GWOT is proposed as follows

$$D = \left| \boldsymbol{C} \cdot \boldsymbol{X}_p(k) - \boldsymbol{X}(t) \right| \tag{15}$$

$$\boldsymbol{X}(k+1) = \boldsymbol{X}_p(k) - \boldsymbol{A} \cdot \boldsymbol{D} \tag{16}$$

where $\boldsymbol{A}$ and $\boldsymbol{C}$ are vector coefficients and k is the current iteration. $\boldsymbol{X}_p$ and $\boldsymbol{X}$ are the prey and grey wolf vector positions, respectively.

Vectors $\boldsymbol{A}$ and $\boldsymbol{C}$ are determined as

$$\boldsymbol{A} = 2\boldsymbol{a} \cdot \boldsymbol{r}_1 - \boldsymbol{a} \tag{17}$$

$$\boldsymbol{C} = 2 \cdot \boldsymbol{r}_2 \tag{18}$$

The random vectors $\boldsymbol{r}_1$–$\boldsymbol{r}_2$ are selected in [0 1], whereas "a" is decreased linearly from 2→0 for various iterations.

Grey wolves typically detect and encircle the prey. Alpha generally leads the chase. Beta-delta sometimes engage in hunting. However, the maximum (prey) position in abstract search space is unknown. To model the activity of grey wolves hunting mathematically, we believe that the alpha-beta (solution for the best candidate) and delta offer better prediction of possible prey positions. Therefore, the first three best possible solutions are saved and the other search agents (together with omegas) are forced to change their positions with the best search agents.

$$\begin{cases} D_\alpha = \left| C_1 \cdot X_\alpha - X \right| & D_\beta = \left| C_2 \cdot X_\beta - X \right| \\ D_\delta = \left| C_3 \cdot X_\delta - X \right| \end{cases} \tag{19}$$

$$\begin{cases} X_1 = X_\alpha - A_1 \cdot D_\alpha & X_2 = X_\beta - A_2 \cdot D_\beta \\ X_3 = X_\delta - A_3 \cdot D_\delta \end{cases} \tag{20}$$

$$X(k+1) = \frac{(X_1 + X_2 + X_3)}{3} \tag{21}$$

The errors of DC and AC PI controllers are (i) summed (integral), (ii) squared, and (iii) time-weighted, referred to as ITSE, and the objective function is expressed as

$$Cost\ function = \int te^2(t)\,\mathrm{d}t \tag{22}$$

The objective function is defined as a minimization problem to minimize the steady-state errors of PI_1 and PI_2, as follows

$$F = w_1 \times ITSE_1 + w_2 \times ITSE_2 \tag{23}$$

where w_1 and w_2 are the weights of $ITSE_1$ and $ITSE_2$, $ITSE_1$ and $ITSE_2$ are the errors between the reference and actual values and serve as inputs to the terminal and DC PI controllers.

The optimized values of DC PI controller gains (k_{p1}, k_{i1}) are 0.38 and 0.026, as shown in Fig 6b; the optimized values of the terminal voltage PI controller gains (k_{p2}, k_{i2}) are 1.32 and 0.67, respectively. In addition, the best solution obtained for the convergence curve of the GWO cost function is 58.1 in nine iterations and is shown in Fig. 6a.

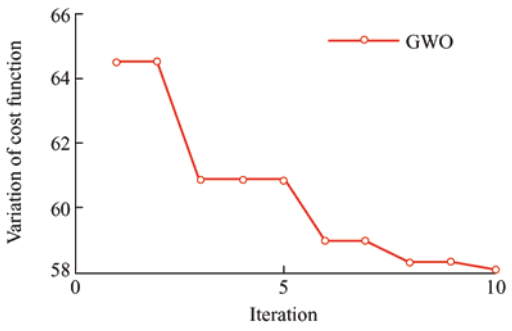

(a) Convergence curve

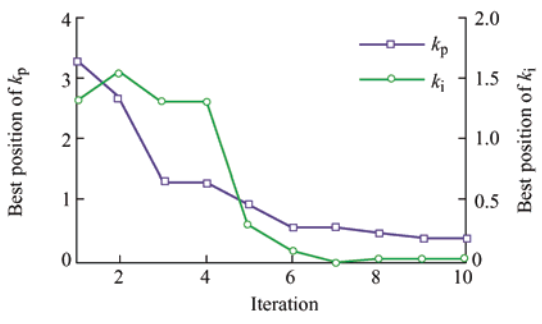

(b) Trajectory of GWO DC-PI gains

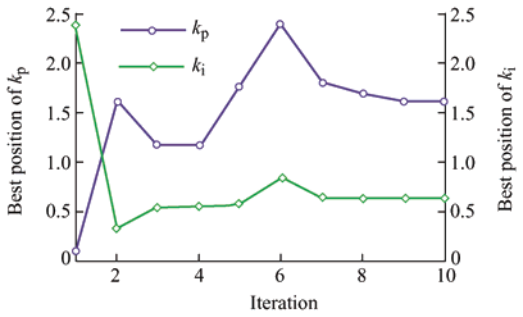

(c) Trajectory of GWO AC-PI gains

Fig. 6 Convergence curve, and DC and AC PI controller gains using the GWOT

6 Results and discussion

The performance of grey wolf-optimized PI gains for UT-based SRF control algorithm for a grid-solar PV system is demonstrated with RL (linear) and power electronic (nonlinear) loads are shown in Fig. 7. The gains of DC and AC bus PI controllers that are acquired from the GWO algorithm are used in this system.

6.1 Performance of a grid-tied PV solar system with linear loads

Fig. 7 shows source grid voltages (V_{sabc}), grid source currents (I_{sabc}), linear load currents (I_{Labc}), controller currents (I_{cabc}), terminal PCC voltage (V_t), DC bus voltage (V_{dc}), solar PV system voltage (V_{pv}), solar PV system current (I_{pv}), load neutral current (I_{Ln}), and source neural current (I_{sn}).

At t=3.8 s, one phase is disconnected and at t=3.9 s the same load is reapplied. However, it was observed that the solar PV source grid currents (I_{sabc}) are free from harmonics and highly balanced owing to the controller operation with improved dynamics. In addition, grid currents and voltages are typically out of phase, which represents voltage regulation. Moreover, it is compensated by the controller. From t=3.75 s to 3.95 s, the voltage of the DC bus (v_{dc}) of the solar PV system is maintained at 800 V by the DC PI controller and the grid terminal voltage (v_{tg}) is maintained at 339.6 V by the ac PI controller. During the aforementioned prescribed time, the load neutral current (i_{Ln}) was present during the unbalance load and it was mitigated by the star/delta transformer which is zero in source neutral current (I_{sn}). The solar PV voltage (V_{pv}) is maintained at 800 V and the solar PV current (I_{pv}) is approximately 3.5 A, illustrating the flow of solar power into the grid with improved dynamics and power quality.

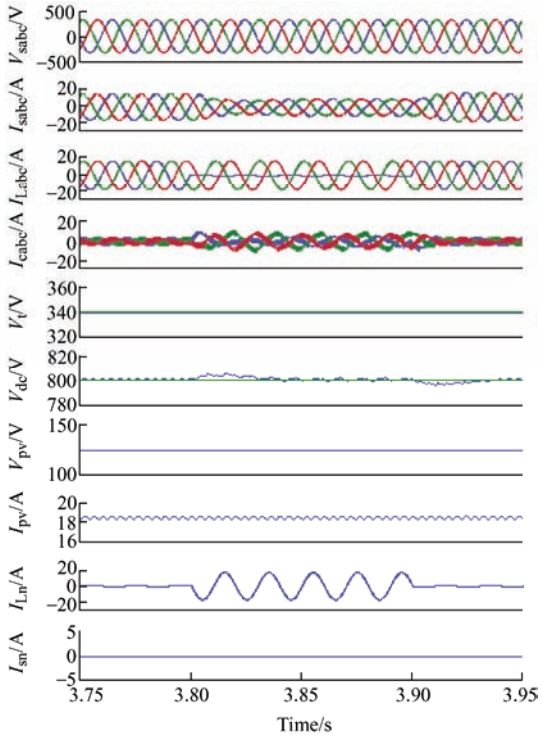

Fig. 7 Performance with linear loads

6.2 Performance of grid-tied PV solar system with nonlinear loads

The performance of grey wolf-optimized gains for the UT-based SRF control algorithm for solar PV systems with the application of nonlinear loads is demonstrated in Fig. 8. The solar PV system source grid voltages (V_{sabc}), source grid currents (I_{sabc}), nonlinear load currents (I_{Labc}), compensator currents (I_{cabc}), terminal PCC voltage (V_t), DC bus voltage (V_{dc}), solar PV system voltage (V_{pv}), current (I_{pv}), source neutral current (I_{sn}), and load neural current (I_{Ln}) are shown in Fig. 8.

At t=3.8 s, one phase is removed and at t=3.9 s the same nonlinear load is reinstated. However, it was observed that the solar PV source grid currents (I_{sabc}) were free from harmonics and balanced, which illustrates the load balancing action of the controller. In addition, grid currents and voltages are usually out of phase, demonstrating the voltage regulation action of the controller. From 3.75 s to 3.95 s, the solar PV dc bus (v_{dc}) maintains a constant value of 800 V and the grid terminal PCC voltage was maintained at 339.6V by both AC and DC PI controllers. As shown in Fig. 8,

from t=3.75 s to 3.97 s, the load neutral current (i_{Ln}) during the unbalanced and nonlinear loads is mitigated by the star/delta transformer and the source neutral current (i_{sn}) is zero. The solar PV current (I_{pv}) is approximately 4.5 A, illustrating the flow of solar power into the grid; the variation V_t, V_{dc}, and the settling time is less, showing improved dynamics and power quality.

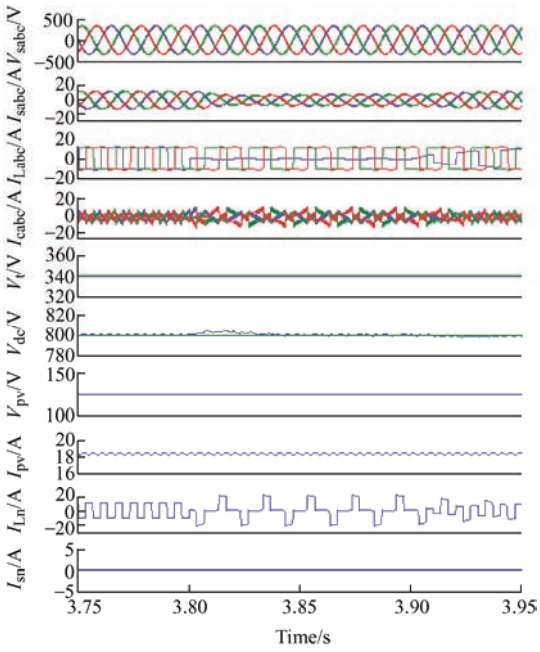

Fig. 8 Performance with nonlinear loads

7 Hardware implementation

The performance of the grid-solar PV system is implemented with linear and nonlinear loads as shown in Figs. 9a-9d with gains acquired from the GWO algorithm.

7.1 Experimental results of systems with linear loads

Fig. 9a shows the grid source voltage of phase "a"(V_{sa}) and grid source currents (I_{sa}, I_{sb}, and I_{sc}). Fig. 9b shows the grid source voltage of phase "a" (V_{sa}) and load currents (I_{La}, I_{Lb}, and I_{Lc}). Fig. 9c shows the grid source voltage of phase "a" (V_{sa}) and compensator currents (I_{ca}, I_{cb}, and I_{cc}), Fig. 9d shows the grid source voltage of phase "a" (V_{sa}), grid current of phase "a" (I_{sa}), load current of phase "c" (I_{Lc}), and compensator current of phase "c" (I_{cc}). Based on observations, whether a linear load is balanced or unbalanced, the source current is balanced and sinusoidal.

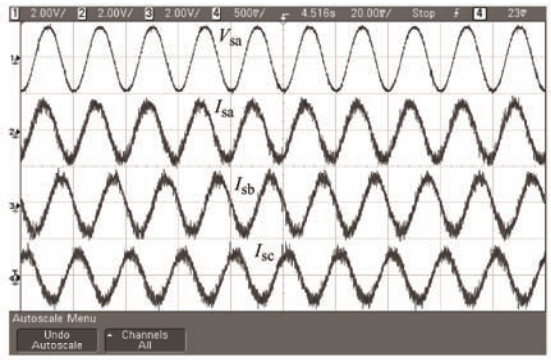

(a) Grid source voltage and current of phase "a"

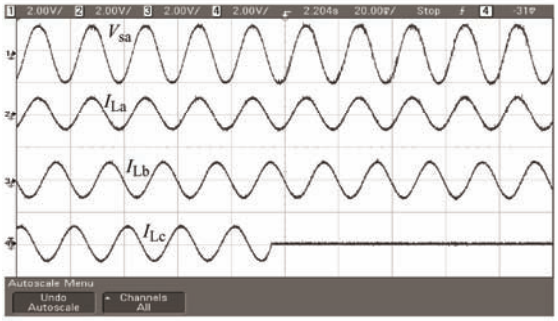

(b) Grid source voltage of phase "a" and load currents

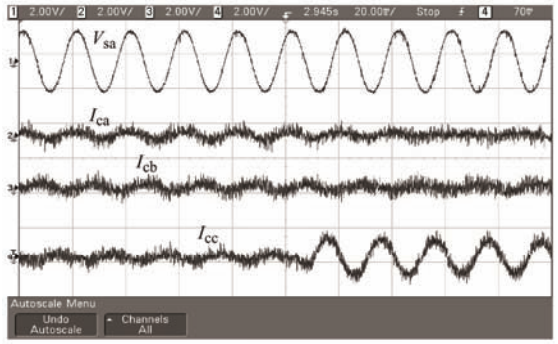

(c) Grid source voltage of phase "a" and compensator currents

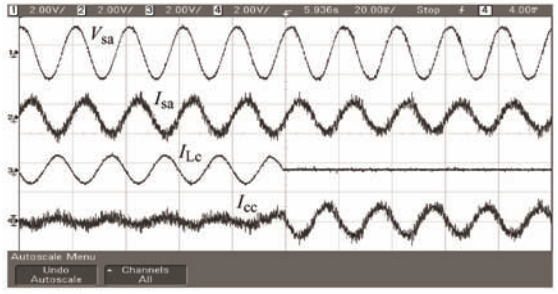

(d) Grid source voltage, grid source current of phase "a" load current, and compensator of phase "c"

Fig. 9 Experimental results with linear loads

7.2 Experimental results of systems with nonlinear loads

Fig. 10a shows the grid source voltage of phase "a" (V_{sa}) and grid source currents (I_{sa}, I_{sb}, and I_{sc}), Fig. 10b shows the grid source voltage of phase "a" (V_{sa}) and load currents (I_{La}, I_{Lb}, and I_{Lc}), Fig. 10c shows the grid source voltage of phase "a" (V_{sa}) and compensator currents (I_{ca},

I_{cb}, and I_{cc}), Fig. 10d shows the grid source voltage of phase "a" (V_{sa}), the grid current of phase "a" (I_{sa}), load current of phase "b" (I_{Lb}), and load neutral current (I_{Ln}). Based on observations, whether the nonlinear load is balanced or unbalanced, the source current is balanced and sinusoidal and when the load is unbalanced, the load neutral current changes.

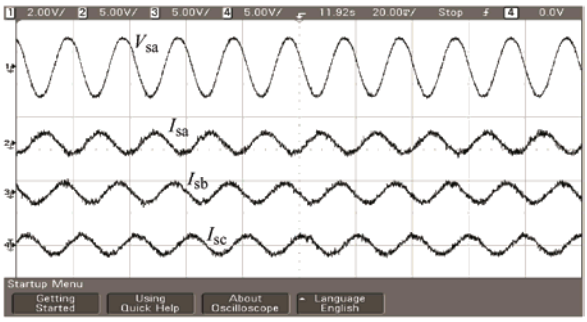

(a) Grid source voltage and current of phase "a"

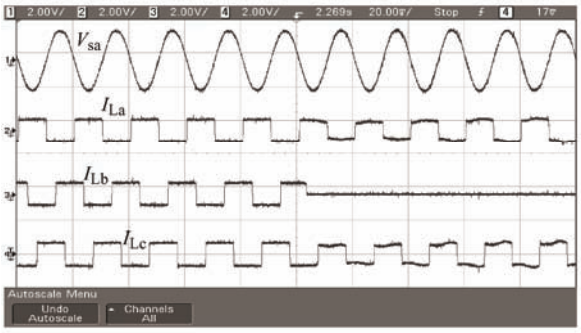

(b) Grid source voltage of phase "a" and load currents

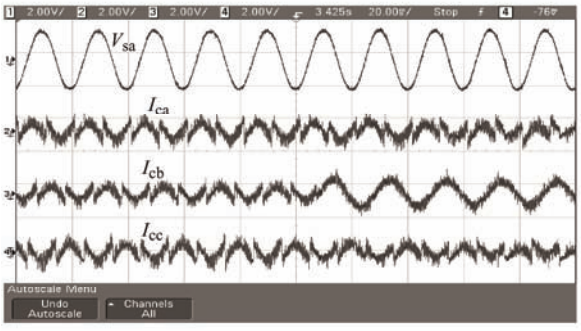

(c) Grid source voltage of phase "a" and compensator currents

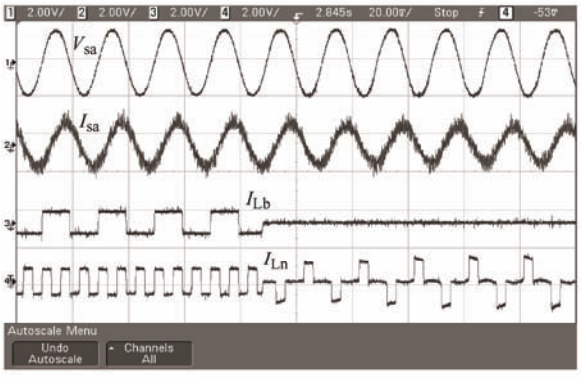

(d) Grid source voltage, grid source current of phase "a" load current(I_{Lb}), and load neutral current(I_{Ln})

Fig. 10 Experimental results with linear loads

The fundamental components of the harmonic spectrum of the voltage source of the solar grid (V_s), grid source current (i_s), and nonlinear load current (i_L) are shown in Figs. 11a-11c. The total harmonic distortion (THD) of the terminal voltage of the solar grid is 2.11%, the grid source current is 3.45%, and the load current has a %THD of 46.45 which is well within IEEE 519 and IEC standards.

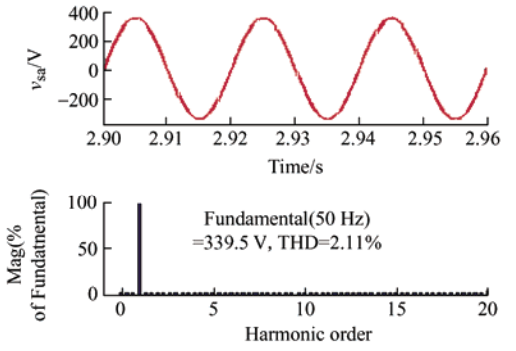

(a) Solar-grid voltage of phase "a"

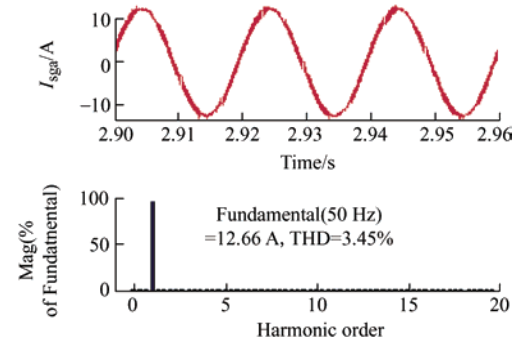

(b) Solar-grid current of phase "a"

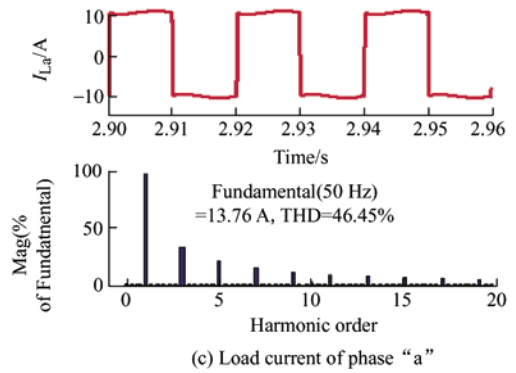

(c) Load current of phase "a"

Fig. 11 (a, b, and c) show the harmonic band of the solar-grid voltage of phase "a," solar-grid current of phase "a," and load current of phase "a."

8 Conclusions

The performance of a grid-connected solar PV system using grey wolf-optimized gains in a UT-based SRF control algorithm was found to offer load balancing, reactive power compensation, and removal of

harmonic currents with the application of linear and nonlinear loads. The proposed GWO algorithm can be used for quick estimation of K_p and K_i gains of PI controllers. The results of the grid-tied solar PV system demonstrate that the UT-based SRF control algorithm is simple, effective, and robust. Moreover, it compensates for power quality problems and improves system dynamics. The waveforms of the grid-connected solar PV system output indicate that sensed DC bus voltage and grid PCC voltage is maintained at 800 V and 339.6 V, respectively. The THD of AC voltage and currents in the solar grid is well within IEC and IEEE 519 standards.

References

[1] L R Foster, M Ghassemi, A Cota. Solar energy renewable energy and the environment. Boca Raton: CRC Press, 2010.

[2] D J Murphy, B L O'Connor, D T Mayhorn, et al. Alternative water resources for utility-scale solar energy development. *Energy Procedia*, 2014, 49: 2501-2511.

[3] J Arillaga, N R Wattson, S Chen. Power system quality assessment. New York: Wiley, 2000.

[4] R C Dugan, M F Mc Granaghan, H W Beaty. Electric power systems quality. 2nd ed. New York: McGraw Hill, 2006.

[5] A Moreno-Munoz. Power quality: Mitigation technologies in a distributed environment. London: Springer-Verlag London Limited, 2007.

[6] Electromagnetic Compatibility (EMC)—Part 3: Limits-Section 2: Limits for Harmonic Current Emissions, IEC1000-3-2 Document 1st edition, 1995.

[7] IEEE Recommended Practices and Requirements for Harmonics Control in Electrical Power Systems, IEEE Std. 519, 1992.

[8] S Bhattacharya, D Diwan. Synchronous frame based controller implementation for a hybrid series active filter system. *Proc. IEEE Industrial Applications Society Meeting*, 1995: 2531-2540.

[9] B N Singh, B Singh, A Chandra, et al. Design and digital implementation of active power filters with power balance theory. *IEE Proceedings - Electric Power Applications*, 2005, 152(5): 1149-1160.

[10] G Bhuvaneswari, M G Nair. Design, simulation, and analog circuit implementation of a three-phase shunt active filter using the IcosΦ algorithm. *IEEE Transaction on Power Delivery*, 2008, 23(2): 1222-1235.

[11] R I Bojoi, L R Limongi, D Roiu, et al. Enhanced power quality control strategy for single-phase inverters in distributed generation systems. *IEEE Transactions on Power Electronics*, 2011, 26(3): 798-806.

[12] J Bangarraju, V Rajagopal, A Jayalaxmi. Unit template synchronous reference frame theory based control algorithm for DSTATCOM. *Journal of Institution of Engineers*, 2014, 95(2): 135-141.

[13] A I Bratcu, I Munteanu, S Bacha, et al. Cascaded DC-DC converter photovoltaic systems: Power optimization issues. *IEEE Transactions on Industrial Electronics*, 2011, 58(2): 403-411.

[14] M A Ghasemi, A Ramyar, H Iman-Eini. MPPT method for PV systems under partially shaded conditions by approximating I-V curve. *IEEE Transactions on Industrial Electronics,* 2018, 65(5): 3966-3975.

[15] C C Hua, Y H Fang, C J Wong. Improved solar system with maximum power point tracking. *IET Renewable Power Generation*, 2018, 12(7): 806-814.

[16] S Mirjalili, S M Mirjalili, A Lewis. Grey wolf optimizer. *Advances in Engineering Software*, 2014, 69: 46-61.

[17] X Li, K M Luk. The grey wolf optimizer and its applications in electromagnetics. *IEEE Transactions on Antennas and Propagation*, 2020, 68(3): 2186-2197.

[18] K Rashidi, S M Mirjalili, H Taleb, et al. Optimal design of large mode area photonic crystal fibers using a multi-objective gray wolf optimization technique. *Journal of Lightwave Technology*, 2018, 36(23): 5626-5632.

[19] M A Elgendy, B Zahawi, D J Atkinson. Assessment of the incremental conductance maximum power point tracking algorithm. *IEEE Transactions on Sustainable Energy*, 2013, 4(1): 108-117.

Veramalla Rajagopal received his AMIE (Electrical) degree from the Institution of Engineers (India), his M.Tech. degree from the Uttar Pradesh Technical University, India, and his Ph.D. degree from the Indian Institute of Technology (IIT), Delhi. He is currently working as a Professor of Electrical and Electronics Engineering at Kakatiya Institute of Technology and Science, Warangal, Telangana, India. His areas of interest include power electronics and drives, renewable energy generation and applications, flexible AC transmission system, and power quality. He holds one Indian patent, has authored 31 international and national journals articles, and has presented at 35 IEEE and national conferences in India and abroad. He is a Life Member of the Indian Society for Technical Education (ISTE) and a Fellow of Institution of Engineers (India).

Danthurthi Sharath received his diploma (Electrical and Electronics) from JN Government Polytechnic, Hyderabad, his B.Tech. degree from JNTU, Manthani, and his M.Tech. from Kakatiya Institute of Technology and Sciences, Warangal. He is currently working as an Assistant Professor of Electrical and Electronics Engineering at Warangal institute of Technology and Sciences, Warangal, Telangana. His areas of interest include power electronics and flexible AC transmission, and power quality and hybrid electric system.

Gundeboina Vishwas received his B.Tech. degree in Electrical and Electronics Engineering from JNTU College of Engineering, Jagtial, India in 2017, and his M.Tech. degree in Power Electronics from Kakatiya Institute of Technology and Sciences, India in 2020. He is currently pursuing his Ph.D. degree in the Department of Electrical Engineering, Sardar Vallabhbhai National Institute of Technology, Surat, India. His research interests include power electronics and drives, multilevel inverters, induction machines, battery management systems, and power quality.

Jampana Bangarraju received the B.Tech. degree in Electrical and Electronics Engineering from A.S.R College of Engineering, Tanuku in 2004, and M.Tech. degree from JNTU, Hyderabad in 2007. He is currently working as Associate Professor in B. V. Raju Institute of Technology, Narsapur, Telangana, India. His areas of interest include power electronics and drives, power quality, FACTS, and artificial neural networks. He is currently pursuing a Ph.D. degree at the Department of Electrical Engineering, JNTU, Hyderabad, India. He is a Life Member of the Indian Society for Technical Education (ISTE) and Member of the Institute of Electrical and Electronics Engineers.

Sabha Raj Arya (S'09-M'19) received his B.E. degree in Electrical Engineering from Government Engineering College, Jabalpur in 2002, M.T. degree in Power Electronics from Motilal National Institute of Technology, Allahabad in 2004, and Ph.D. degree in Electrical Engineering from the Indian Institute of Technology (IIT) Delhi, New Delhi, India in 2014. He joined as an Assistant Professor in the Department of Electrical Engineering, Sardar Vallabhbhai National Institute of Technology, Surat. In January 2019, he was promoted to Associate Professor in the same institution. His fields of interest include power electronics, power quality, design of power filters and distributed power generation. He has received two national awards for his research work: INAE Young Engineer Award from the Indian National Academy of Engineering and the POSOCO Power System Award from the Power Grid Corporation of India in 2014. He has also received the Amit Garg Memorial Research Award in 2014 from IIT Delhi for high impact journal publications during the 2013–2014 session. He has published more than 100 research papers in international journals and conferences in the field of electrical power quality.

He also serves as an Associate Editor for the IET (UK) Renewable Power Generation.

Challa Venkatesh received his B.Tech. (Electrical Engineering) and M.Tech. (Power Electronics) degrees from University Visvesvaraya College of Engineering, Bangalore, India, and his Ph.D. degree from National Institute of Technology & Science, Warangal, India. He is currently working as a Professor of Electrical and Electronics Engineering, Kakatiya Institute of Technology and Science, Warangal, Telangana, India. His areas of interest include power quality analysis, power electronics and drives, and renewable energy generation and applications. He has authored 14 international and national journal articles and has presented at 20 IEEE and national conferences in India and abroad. He is a Life Member of the Indian Society for Technical Education (ISTE).